A METHOD FOR PROPAGATING UNCERTAINTIES OF THE TOP OF ATMOSPHERE SENTINEL-2 MEASUREMENTS TO BOTTOM OF ATMOSPHERE REFLECTANCE FOR AQUATIC APPLICATIONS

Nicolas THOMAS[*], *Marc LENNON*[*], *Céline DANILO*[*], *Guillaume SICOT*[**], *Mohamed ALI GHANNAMI*[**], *Sophie LOYER*[***]

[*]: Hytech-imaging, Brest, France
[**]: ENSTA Bretagne - M3 team - Lab-STICC - UMR CNRS 6285, Brest, France
[***]: Shom, Brest, France

ABSTRACT

A method is proposed to analytically propagate the measurement uncertainties of multispectral or hyperspectral satellite sensors from the top of the atmosphere to the surface as well as through the correction of specular reflections from the sun, in a maritime application context. The method is applied to the Sentinel2-MSI sensor and validated by a Monte Carlo technique. The resulting surface reflectance uncertainties can again be propagated to subsequent treatment processes such as the inversion of the radiative transfer model in the water column.

***Index Terms*—** remote sensing, uncertainty, Sentinel-2, atmospheric correction, surface reflectance, sunglint

1. INTRODUCTION

The growing volume of high-resolution multispectral satellite sensor data available has paved the way for the development of many applied methods of image processing and cartography, for a variety of application fields, whether in agronomy, forestry or coastal environmental monitoring.

To enable their use by a large number of end-users, these methods need to be able to quantify the uncertainty in the products derived from the satellite images they produce.

Even if Monte-Carlo methods can propagate the uncertainties of the sensor measurement through the processing chains to derived products, their computational complexity makes them unsuitable for the large volumes of data to be processed which are generated daily by satellite constellations.

Therefore, in this paper we propose a method for analytically propagating the uncertainty on the sensor measurement at the top of the atmosphere (TOA) through the atmospheric correction process to the reflectance at the bottom of the atmosphere (BOA). In an aquatic application context, we propose an additional propagation step through the surface effects correction process to the water reflectance. This method is a first step before the propagation of uncertainties through the extraction of derived products such as bathymetry.

Since, to our knowledge, the Sentinel-2 MultiSpectral Instrument (MSI) sensor is, among the metric resolution multispectral sensors, the one with the most advanced sensor uncertainty characterization, the method is based on data from this sensor, and more particularly in a sea area in order to implement sun surface effects correction. Nevertheless, the method can be applied on other sensors, provided their measurement uncertainty is known.

2. SENTINEL 2 MSI TOA REFLECTANCE

The input data of our method is the observed spectral reflectance at the TOA, $\rho^*_{toa_{i,j}}(\lambda)$ for the image pixel indices i, j and for the band averaged wavelength λ. Because the proposed method works independently for each spatial pixel i, j they will we omitted in the following paragraphs. Also, the first steps of the method are similar for every λ thus we will also omit it during these steps.

For the Sentinel-2 MSI sensor, $\rho^*_{toa_{i,j}}(\lambda)$ is made available on the Copernicus Open Access Hub with the Level-1C product from which the image presented in the validation section is selected.

3. SENTINEL 2 MSI TOA REFLECTANCE UNCERTAINTY

The TOA reflectance uncertainty of Sentinel-2 MSI data is not yet a standard product delivered by Copernicus, however a major effort has been made to characterize it as part of the development of the Radiometric Uncertainty Tool (RUT) [1]. The noise model used in RUT, which is used in our method, includes 12 components which are recalled in TABLE I.:

TABLE I. COMPONENTS OF THE UNCERTAINTY IN RUT

Instrument noise	Out-of-Field Stray-Light Systematic Part
Out-of-Field Stray-Light Random Part	Crosstalk
Analog-to-Digital Converter (ADC)	Quantisation, Dark Signal Stability
Non-Linearity and Non-Uniformity Knowledge	Diffuser Reflectance Absolute Knowledge
Diffuser Reflectance	Angular Diffuser Knowledge—Cosine Effect Temporal Knowledge
Stray-Light in Calibration Mode—Residual	Image Quantisation

From these contributions of heterogeneous types (Gaussian noise, uniform noise, uncorrected systematic errors) an overall uncertainty, relative to the measurement, is determined for each pixel and each band of the image by following the Guide to the Expression of Uncertainty in Measurement [2] recommendations as far as possible. Unlike the processing performed in RUT, where the uncertainty is finally expressed as a percentage of the 8-bit reflectance, in order to maintain the accuracy required for its propagation, we keep here the uncertainty, $U_{\rho^*_{toa}}$ as a floating reflectance value.

At certain stages in the propagation process, assumptions on the statistical law of ρ^*_{toa} uncertainty will have to be made. Despite, as explained here above, the uncertainty on Sentinel-MSI is well described with several components characterized by heterogeneous statistical laws, this is not the case for all sensors. Thus, in order to build a generic method, we formulate the assumption that the uncertainty on ρ^*_{toa} which is quantified by $U_{\rho^*_{toa}}$ is well represented by a spectrally decorrelated centered gaussian law. The possibility of lifting the decorrelation assumption is mentioned in the conclusion.

4. ATMOSPHERIC CORRECTION

In order to obtain the estimated surface reflectance at bottom of atmosphere $\hat{\rho}_s$, we need to correct for the effects of the atmosphere on ρ^*_{toa} . We used for this the method presented in [3]:

$$\hat{\rho}_s = \frac{1}{\frac{T}{(\rho^*_{toa}-\rho_a)}+S} \quad (1)$$

In (1) T is the atmospheric transmittance including both scattering and gas absorption components along the sun–sensor path, ρ_a and S are the atmospheric reflectance and spherical albedo incorporating the coupled effects of gas absorption. T, ρ_a and S are obtained using the 6S (Second Simulation of a Satellite Signal in the Solar Spectrum – [4] and [5]) radiative transfer code. Inputs of this code are the solar $\theta_s$and sensor view $\theta_v$zenith angles to the scene, the atmospheric profile model, the aerosol model, the aerosol optical thickness (AOT) at 550 nm. Uncertainty on these inputs is not considered here because their analytical propagation through the direct radiative transfer model in T, ρ_a and S is an unresolved issue.

5. PROPAGATING $U_{\rho^*_{toa}}$ IN THE ATMOSPHERIC CORRECTION

On a measured sample, ρ^*_{toa} is composed of the exact TOA reflectance ρ_{toa} and the measurement error $\varepsilon_{\rho_{toa}}$:

$$\rho^*_{toa} = \rho_{toa} + \varepsilon_{\rho_{toa}} \quad (2)$$

With the assumption of a normal centered law for the measurement error, on a series of samples, the values of $\varepsilon_{\rho_{toa}}$are statistically characterized by $U_{\rho^*_{toa}}$ which is the standard deviation in this context.

Introducing $\varepsilon_{\rho_{toa}}$ in (1) enables developing with a first order Taylor development:

$$\hat{\rho}_s = \frac{1}{\frac{T}{\left(\rho_{toa}+\varepsilon_{\rho_{toa}}-\rho_a\right)}+S} \quad (3)$$

$$\hat{\rho}_s = \frac{1}{\frac{T}{(\rho_{toa}-\rho_a)}+S} + \frac{T}{\left(T+S(\rho_{toa}-\rho_a)\right)^2}\varepsilon_{\rho_{toa}} + o\left(\varepsilon_{\rho_{toa}}\right) \quad (4)$$

Then if ρ_s is the exact surface reflectance, we have:

$$\rho_s = \frac{1}{\frac{T}{(\rho_{toa}-\rho_a)}+S} \quad (5)$$

And thus:

$$\hat{\rho}_s = \rho_s + \frac{T}{\left(T+S(\rho_{toa}-\rho_a)\right)^2}\varepsilon_{\rho_{toa}} + o\left(\varepsilon_{\rho_{toa}}\right) \quad (6)$$

Because practically ρ_{toa} is not available for computation, still with a Taylor development we show that we also have:

$$\hat{\rho}_s = \rho_s + \frac{T}{\left(T+S(\rho^*_{toa}-\rho_a)\right)^2}\varepsilon_{\rho_{toa}} + o\left(\varepsilon_{\rho_{toa}}\right) \quad (7)$$

From (7) and owing to the assumption that ρ^*_{toa} uncertainty is spectrally decorelated we have a good approximate, at first order, of the uncertainty on $\hat{\rho}_s$:

$$U_{\hat{\rho}_s} = \alpha_U U_{\rho^*_{toa}} \quad (8)$$

$$\alpha_U = \frac{T}{\left(T+S(\rho^*_{toa}-\rho_a)\right)^2} \quad (9)$$

6. PROPAGATING $U_{\hat{\rho}_s}$ IN THE CORRECTION OF THE SUNGLINT

For coastal applications, such as bottom mapping or bathymetric measurements, a common pre-processing before working on water reflectance is removing the specular reflections from the sun (sunglint).

For images of metric spatial scale, one of the methods consists in using a spectral band for which the water reflectance is assumed to be 0 in the Near Infra Red (NIR) or Short Wave Infra Red (SWIR) spectral domain (assumption made if turbidity is not too high), and therefore including only the reflectance due to the sunglint, to subtract it from the other spectral bands by means of an adapted weighting. Here we use such a method as presented in [6]. If we write $\rho_g(\lambda)$the reflectance of the glint at wavelength λ, that we reintroduce for this spectrally dependent method, then from [6] we have:

$$\rho_g(\lambda) = \rho_s(\lambda_{ref}) \frac{T_{dir}(\lambda)}{T_{dir}(\lambda_{ref})} \frac{r(\theta,\lambda)}{r(\theta,\lambda_{ref})} \quad (10)$$

where $\lambda_{ref}$is the averaged wavelength of the reference band, $T_{dir}$is the two-way direct transmittance of the atmosphere which is available from 6S. $r(\theta,\lambda)$ is the Fresnel reflectance coefficient for air-incident rays at wavelength λ depending on θ_s, θ_v, the relative azimuth angle $\Delta\Phi$ and $n_w(\lambda)$ the band averaged refractive index of water with respect to air at wavelength λ, as shown in [6].

Now, let's write $\hat{\rho}_g(\lambda)$ the estimate of the sunglint reflectance at wavelength λ, composed of the exact sunglint reflectance $\rho_g(\lambda)$ and the error and this estimate $\varepsilon_{\rho_g}(\lambda)$:

$$\hat{\rho}_g(\lambda) = \rho_g(\lambda) + \varepsilon_{\rho_g}(\lambda) \quad (11)$$

Following (7) and owing to the linear relation in (10) applied to the estimate of surface reflectance $\hat{\rho}_s(\lambda)$,at first order we have:

$$\varepsilon_{\rho_g}(\lambda) = \frac{T_{dir}(\lambda)}{T_{dir}(\lambda_{ref})} \frac{r(\theta,\lambda)}{r(\theta,\lambda_{ref})} \alpha_U(\lambda_{ref}) \varepsilon_{\rho_{toa}}(\lambda_{ref}) \quad (12)$$

With $\hat{\rho}_w(\lambda)$ the estimated water surface reflectance after sunglint removal, we have like in (11):

$$\hat{\rho}_w(\lambda) = \rho_w(\lambda) + \varepsilon_{\rho_w}(\lambda) \quad (13)$$

And we practically compute it for each band averaged λ with:

$$\hat{\rho}_{w(\lambda)} = \hat{\rho}_{s(\lambda)} - \hat{\rho}_{g(\lambda)} \quad (14)$$

Finally, from (7), (12) and (14) we have:

$$\varepsilon_{\rho_w}(\lambda) = \alpha_u(\lambda)\varepsilon_{\rho_{toa}}(\lambda) - \frac{T_{dir}(\lambda)}{T_{dir}(\lambda_{ref})} \frac{r(\theta,\lambda)}{r(\theta,\lambda_{ref})} \alpha_u(\lambda_{ref}) \varepsilon_{\rho_{toa}}(\lambda_{ref}) \quad (15)$$

Owing to the assumption that the uncertainty on $\rho^*_{toa}(\lambda)$ is well represented by a spectrally decorrelated centred gaussian law, from (15) we have the uncertainty in the surface reflectance of water after removal of sunglint $U_{\hat{\rho}_w}(\lambda)$:

$$U_{\hat{\rho}_w}(\lambda) = \sqrt{\alpha_u^2(\lambda) U^2_{\rho^*_{toa}}(\lambda) + \left(\frac{T_{dir}(\lambda)}{T_{dir}(\lambda_{ref})} \frac{r(\theta,\lambda)}{r(\theta,\lambda_{ref})}\right)^2 \alpha_u^2(\lambda_{ref}) U^2_{\rho^*_{toa}}(\lambda_{ref})} \quad (16)$$

7. RESULTS AND VALIDATIONS USING A MONTE-CARLO METHOD

The results are presented on a subset of a Level-1C image from Sentinel 2B MSI in South-East of Martinique dated 2020/09/05 (Fig. 1).

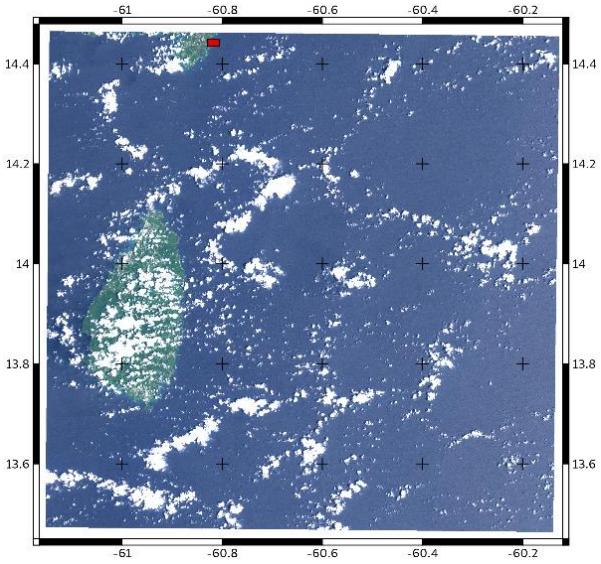

Fig. 1. Position of the area of interest southeast of Martinique, north of the tile Level-1C S2B_MSIL1C_20200905T143729_N0209_R096_T20PQA_20200905T162936

True color overviews of this test area are presented for the TOA reflectance ρ^*_{toa} in Fig. 2, and for the water reflectance after sunglint removal $\hat{\rho}_w$ in Fig. 3.

In order to present the calculated uncertainties, we represent them spectrally in Fig. 4 by the ratio $\frac{\rho}{U_\rho}$ for the 5 sites shown in Fig. 2. The figure shows the decrease of this ratio during the steps of atmospheric correction and then sunglint removal. The ratio is particularly low on the whole spectrum for sites 2 and 3 located on dark backgrounds. Site 4, a priori deeper than site 3, nevertheless presents a better ratio because it is located on a lighter background.

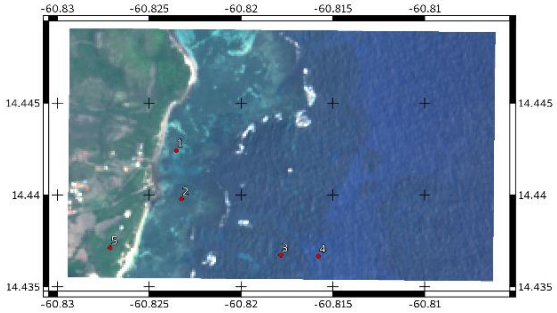

Fig. 2. True color overview (bands 4, 3 and 2, respectively at 665nm, 559nm and 492nm) of ρ^*_{toa} on the test area. Five sample sites are identified.

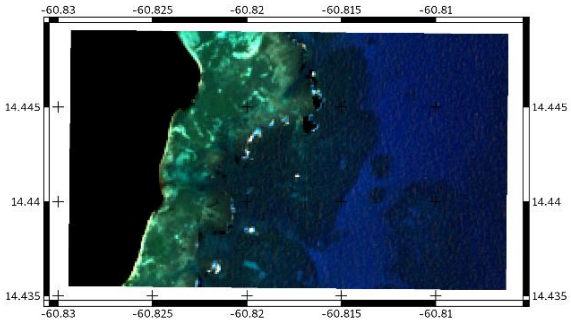

Fig. 3. True color overview (bands 4, 3 and 2, respectively at 665nm, 559nm and 492nm) of $\hat{\rho}_w$ on the test area.

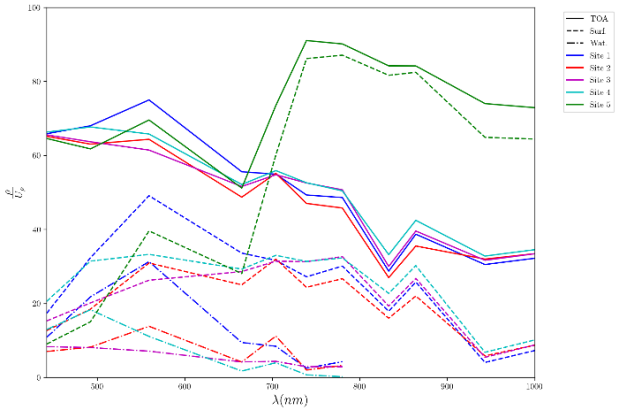

Fig. 4. $\frac{\rho}{U_\rho}$ curves between 442nm and 1000nm for the 3 reflectances ρ^*_{toa}, $\hat{\rho}_s$ and $\hat{\rho}_w$, for 5 sites selected on the test area. Site 5 is not on water thus $\hat{\rho}_w$ is not available for this site. $\hat{\rho}_w$ is not computed after 780nm.

In order to validate these results, we use a Monte-Carlo method. Here the measured TOA reflectance ρ^*_{toa} is considered as the exact TOA reflectance. Thus, a simulated error $\varepsilon_{\rho_{toa,si}}$ is randomly generated with a normal centered law of standard deviation $U_{\rho^*_{toa}}$. We then produce the simulated measurement of TOA reflectance:

$$\rho^*_{toa,si} = \rho^*_{toa} + \varepsilon_{\rho_{toa,si}} \quad (17)$$

$\rho^*_{toa,si}$ is then used to compute the simulated estimate of $\hat{\rho}_{s,si}$ with (3) and the equivalent after sunglint removal $\hat{\rho}_{w,si}$ using (10) and (14). The simulated error on the surface reflectance is:

$$\varepsilon_{\hat{\rho}_{s,si}} = \hat{\rho}_{s,si} - \hat{\rho}_s \quad (18)$$

The simulated error on the surface reflectance is:

$$\varepsilon_{\hat{\rho}_{w,si}} = \hat{\rho}_{w,si} - \hat{\rho}_w \quad (19)$$

The operation is reproduced 5000 times for every pixels of the test image which enables computing means on $\bar{\varepsilon}_{\hat{\rho}_{s,si}}$ and $\bar{\varepsilon}_{\hat{\rho}_{w,si}}$ and standard deviations $\sigma_{\varepsilon_{\hat{\rho}_{s,si}}}$ and $\sigma_{\varepsilon_{\hat{\rho}_{w,si}}}$. Normality of the simulated samples is confirmed graphically using a normal fit for all spectral bands on some spatial pixels. Fig. 5 show an example on site 1 for band 3 at 559nm.

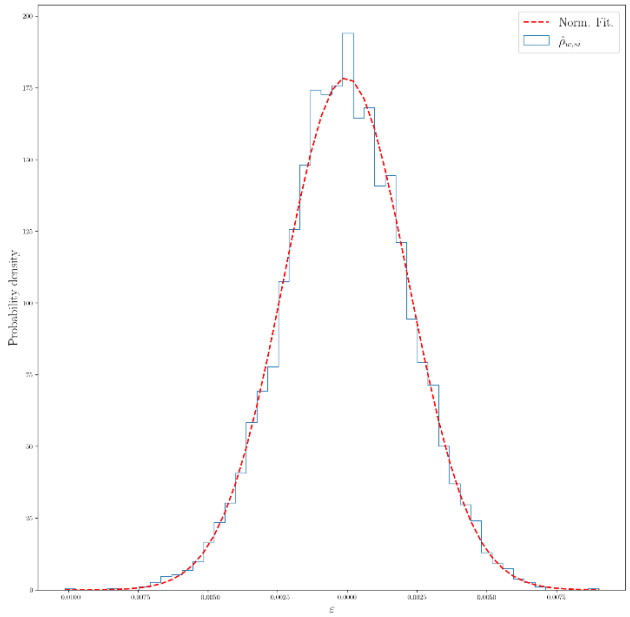

Fig. 5. Normal fit of the histogram of the $\varepsilon_{\hat{\rho}_{s,si}}$ samples on site 1 for band 3 at 559nm

A spatial mean of $\bar{\varepsilon}_{\hat{\rho}_{s,si}}$ and $\bar{\varepsilon}_{\hat{\rho}_{w,si}}$, on the 37500 pixels of the test area, is computed for each spectral band, the very low values presented in TABLE II show that, as expected the Monte-Carlo simulation converges to a centered normal distribution. We can then write for the simulated uncertainty:

$$U_{(\hat{\rho}_s),si} = \sigma_{\varepsilon_{\hat{\rho}_{s,si}}} \quad (20)$$

$$U_{(\hat{\rho}_w),si} = \sigma_{\varepsilon_{\hat{\rho}_{w,si}}} \quad (21)$$

TABLE II. SPATIAL STATISTICS ON THE MONTE-CARLO RESULTS

Band	λ(nm)	Spatial mean $\bar{\varepsilon}_{\hat{\rho}_{s,si}}$	Spatial std. $\Delta U_{\hat{\rho}_s}$	Spatial mean $\bar{\varepsilon}_{\hat{\rho}_{w,si}}$	Spatial std. $\Delta U_{\hat{\rho}_w}$
1	442	-1.60e-06	1.00e-02	-1.52e-06	9.99e-03
2	492	-6.78e-07	9.95e-03	-6.05e-07	9.95e-03
3	559	-2.42e-07	1.00e-02	-1.58e-07	1.00e-02
4	665	-1.18e-07	1.00e-02	-2.72e-08	1.00e-02
5	704	-8.14e-08	1.00e-02	6.91e-08	9.99e-03
6	739	-1.23e-07	9.94e-03	2.92e-08	9.98e-03
7	780	-2.04e-08	9.99e-03	1.33e-07	1.00e-02
8	833	-9.57e-08	1.00e-02	N/A	N/A
9	864	-1.23e-07	1.00e-02	N/A	N/A
10	943	-1.84e-07	1.01e-02	N/A	N/A
11	1610	-1.54e-07	9.98e-03	N/A	N/A
12	2186	-1.06e-07	9.98e-03	N/A	N/A

And the relative difference between the analytic uncertainties and Monte-Carlo uncertainties are:

$$\Delta U_{\hat{\rho}_s} = \frac{U_{\hat{\rho}_s,si} - U_{\hat{\rho}_s}}{U_{\hat{\rho}_s}} \quad (22)$$

$$\Delta U_{\hat{\rho}_w} = \frac{U_{\hat{\rho}_w,si} - U_{\hat{\rho}_w}}{U_{\hat{\rho}_w}} \quad (23)$$

A spatial standard deviation of $\Delta U_{\hat{\rho}_s}$and $\Delta U_{\hat{\rho}_w}$ is computed for each spectral band, the values near 0.01 presented in TABLE II agree with the expected standard deviation for 5000 samples which can be estimated with:

$$\frac{1}{\sqrt{2(5000-1)}} \cong 0.01 \quad (24)$$

Thus, the Monte-Carlo simulation converges to the analytical solution for $U_{\hat{\rho}_s}$ and $U_{\hat{\rho}_w}$.

8. CONCLUSION AND FURTHER WORK

This paper describes a method to analytically propagate the reflectance measurement uncertainties of multispectral or hyperspectral satellite sensors from the top of the atmosphere to the surface as well as through the correction of specular reflections from the sun, in a maritime application context. The first order analytical method agrees with the results of a Monte Carlo technique when applied to normal, centered, spectrally decorrelated input TOA uncertainties. This was shown with Sentinel-2 MSI input data. The resulting surface reflectance uncertainties can again be propagated to subsequent treatment processes such as the inversion of the radiative transfer model in the water column. The next work will consist in using recent advances on the characterization of the spectral and spatial covariances of TOA uncertainties [7] in order to integrate them in the developed propagation model. We believe that the spectral covariances of the TOA uncertainty could induce a reduction of the output uncertainty variances after the sunglint removal step.

11. REFERENCES

[1] J. Gorroño,N. Fomferra, M. Peters;F. Gascon;C. I. Underwood, N. P. Fox, G. Kirches, C. Brockmann,"A Radiometric Uncertainty Tool for the Sentinel 2 Mission," *Remote Sens.* 9, 178, 2017

[2] JCGM, "Guide to the Expression of Uncertainty in Measurement," Available online: http://www.bipm.org/en/publications/guides/gum.html (accessed on 14 February 2021).

[3] D. R. Thompson, L. Guanter, A. Berk, et al., "Retrieval of Atmospheric Parameters and Surface Reflectance from Visible and Shortwave Infrared Imaging Spectroscopy Data," *Surv Geophys* 40, pp 333–360, 2019

[4] S. Kotchenova, E. Vermote, R. Matarrese, and F. Klemm, Jr., "Validation of a vector version of the 6S radiative transfer code for atmospheric correction of satellite data. Part I: Path radiance," *Appl. Opt.* 45,pp 6762-6774, 2006

[5] S. Kotchenova and E. Vermote, "Validation of a vector version of the 6S radiative transfer code for atmospheric correction of satellite data. Part II. Homogeneous Lambertian and anisotropic surfaces," *Appl. Opt.* 46, pp 4455-4464, 2007

[6] Q. Vanhellemont, "Adaptation of the dark spectrum fitting atmospheric correction for aquatic applications of the Landsat and Sentinel-2 archives," *Remote Sensing of Environment*,Volume 225, pp 175-192, 2019

[7] J. Gorroño, S. Hunt, T. Scanlon, A. Banks, N. Fox, E. Woolliams, C. Underwood, F. Gascon, M. Peters, N. Fomferra, Y. Govaerts, N. Lamquin, V. Bruniquel, "Providing uncertainty estimates of the Sentinel-2 top-of-atmosphere measurements for radiometric validation activities", *European Journal of Remote Sensing*, 51:1, pp 650-666, 2018